Comparison of non-pulsating reflective PPG signals in skin phantom, wearable device prototype, and Monte Carlo simulations

Maximilian Reiser[1], Timm Müller[2], Klaus Flock[2], Oliver Amft[3] and Andreas Breidenassel[4]

***Abstract*— We obtain and compare the non-pulsating part of reflective Photoplethysmogram (PPG) measurements in a porcine skin phantom and a wearable device prototype with Monte Carlo simulations and analyse the received signal. In particular, we investigate typical PPG wavelengths at 520, 637 and 940 nm and source-detector distances between 1.5 and 8.0 mm. We detail the phantom's optical parameters, the wearable device design, and the simulation setup. Monte Carlo simulations were using layer-based and voxel-based structures. Pattern of the detected photon weights showed comparable trends. PPG signal, differential pathlength factor (DPF), mean maximum penetration depth, and signal level showed dependencies on the source-detector distance d for all wavelengths. We demonstrate the signal dependence of emitter and detection angles, which is of interest for the development of wearables.**

I. INTRODUCTION

Photoplethysmogram (PPG) measurements are a non-invasive optical method to obtain a variety of vital signs at the human body [1]. PPG systems comprise a light source and photodiode to detect blood vessel volume changes. For wearable applications, often a reflective PPG measurement is considered, which creates a banana-shaped curve of non-absorbed photons between source and detector [2]. Static absorption (DC level) is caused by tissue, i.e. skin layers and blood. The DC level is an important parameter for estimating the PPG signal quality and for determining further vital parameters, including respiratory frequency and temperature changes [3]. Sensor geometry, including the distance between source and detector, has an important influence on the PPG signal's DC level, i.e. the non-pulsating signal part, and depends on measurement location and anatomy [4], [5]. Furthermore, the source wavelength influences the PPG curve, DC level, and optimal sensor geometry. Considering the optical signal influences, simulation tools are sought that could support designers to create PPG systems.

Monte Carlo (MC) simulations are an established method to analyse photon-tissue interactions [6]. To reduce complexity of the human anatomy, simplified skin models based on one or more homogeneous layers are often used to analyse photon trajectories and their detection [7]. The detected photon weight in simulations is directly related to the DC level in a physical measurement. However, the complexity of human anatomy and unknown optical properties of the skin still limit a transfer from simulations to physical measurements. Thus, a deeper understanding of PPG DC level in relation to system geometry and wavelength is needed.

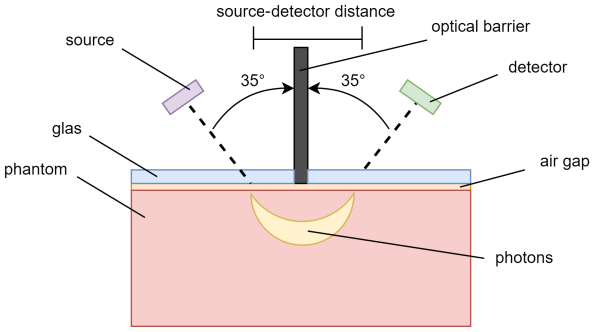

Fig. 1. Illustration of the measurement setup. The source-detector distance d was varied between 2.0 mm and 8.0 mm in 0.2 mm increments. Source and detector were oriented at an angle of 35 °. The phantom was covered by a microscope slide with an optical barrier.

In this paper, we analyse the agreement between physical measurements in a porcine skin phantom and a purpose-built wearable prototype with MC simulations. Porcine skin provides similar optical properties to human skin. Our simulations are based on a previously presented framework [8]. In particular, the paper provides the following contributions:

1) We present laboratory measurements of a homogeneous porcine skin phantom at different wavelengths and source-detector distances. Optical parameters of the phantom and the measurement setup are detailed to compare with MC simulations.
2) We contrast physical measurements of a wearable prototype on the porcine phantom with the laboratory setup measurements and our simulations.

II. METHODOLOGY

To compare physical measurement and MC simulation, we analyse the absorption of a porcine skin phantom for three wavelengths and varying source-detector distances. Initially, the detector DC level was measured in an optical laboratory setup to maintain constant conditions. Measurements were compared against MC simulations, performed using an existing framework [8]. Finally, a purpose-built wearable prototype was used to analyse wavelength and source-detector distances under more variable conditions.

A. Phantom

A microstructered phantom made from epoxy resin [9] was obtained for our analysis. The phantom was designed

[1]M. Reiser is with Faculty of Electrical Engineering, HAW Landshut and Faculty of Engineering, University of Freiburg, Germany
[2]T. Müller and K. Flock are with ASM Osram
[3]O. Amft is with the Faculty of Engineering, University of Freiburg and Hahn-Schickard, Germany
[4]A. Breidenassel is with the Faculty of Electrical Engineering, HAW Landshut, Germany

as a homogeneous structure to simulate optical parameters of porcine skin (see Tab. I). The phantom had a cylindrical shape with a height of 50 mm, a radius of 25 mm, and a polished surface.

B. Laboratory setup and measurements

The source as well the detector were placed in a fixed angle of 35 ° above the phantom with a variable source-detector distance d (see Fig. 1). Source diameter was 0.61 mm and detector diameter 0.55 mm at the surface. The phantom was covered by a microscope glass slide with a thickness of 1 mm. For simulations, an air gap of 0.1 mm was assumed. Direct crosstalk between source and detector across the slide was prevented by an optical barrier.

The source-detector distance d was varied between 2.0 and 8.0 mm in 0.2 mm increments. Thus, the source and detector were placed over the phantom symmetrically. We analysed wavelengths 520, 637, and 940 nm.

We measured the reflected DC level which is comparable with the detected photon weight of the simulation and is named signal level in the following.

C. Monte Carlo Simulations

MC simulations were used to represent photon interactions in tissue. Sensors, glass slide, and optical barrier were implemented as a voxel model to describe their geometrical parameters. The homogeneous phantom was implemented as a layered model to maximise simulation speed.

Absorption coefficient μ_a of tissue determines the reduction of photon weight w while propagating through tissue. Scattering coefficient μ_s describes the probability of photon scattering. Photons were bundled as photon packets and sent into tissue with a statistical weight $w = 1.0$.

First, the photon was sent into the phantom and path length l was determined by a random number ξ (uniformly distributed between 0 and 1) depending on μ_s of the tissue:

$$l = -\frac{\ln(\xi)}{\mu_s}. \tag{1}$$

After travelling the path length l, a part of w was absorbed depending on μ_a by Lambert-Beer's law:

$$w = w \cdot e^{-\mu_a \Delta l}. \tag{2}$$

Subsequently, a scattering event was triggered. Using the Henyey-Greenstein phase function [8], a new scattering angle θ was calculated:

$$p(\theta) = \frac{1}{4\pi} \frac{1-g^2}{(1+g^2-2g\ cos\theta)^{\frac{3}{2}}}, \tag{3}$$

where g is the anisotropy factor. Afterwards a new step length l was determined. If a photon packet encounters a tissue border in between, reflectance R [8] was used to calculate whether the photon packet was reflected or transmitted:

$$R = \begin{cases} \frac{(n_i-n_t)^2}{(n_i+n_t)^2} & \text{if } \theta_i = 0, \\ \frac{1}{2}\left[\frac{sin^2(\theta_i-\theta_t)}{sin^2(\theta_i+\theta_t)} + \frac{tan^2(\theta_i-\theta_t)}{tan^2(\theta_i+\theta_t)^2}\right] & \text{if } 0 < \theta_i < \theta_c, \\ 1 & \text{if } \theta_c < \theta_i < \frac{\pi}{2}, \end{cases} \tag{4}$$

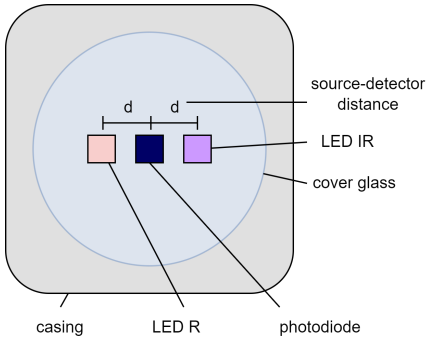

Fig. 2. Illustration of the developed wearable prototype. The source-detector distance d was varied between 1.5, 3.0, 5.0, and 7.0,mm. The sensor system had a cover glass.

where θ_i, θ_t and θ_c are the incident angle, transmission angle, and critical angle. If R was smaller as ξ, the photon packet was transmitted, otherwise reflected. Subsequently, the process continued with updated or the same tissue parameters. The previous steps continued repetitively until $w < 10^{-4}$, or the photon packet hit the phantom surface. The Russian Roulette technique [8] was performed if the former occurred, where the photon packet had a chance of 1:10 to tenfold its weight.

Simulated metrics were the number of photon packets detected w, the average maximum penetration depth, and the average optical pathlength l of photon packets. In scattering tissue, l differs from the source-detector distance d and the geometric pathlength, d. The relationship is quantified by the differential pathlength factor DPF:

$$l = d \times DPF. \tag{5}$$

For non-scattering tissue, the Lambert-Beer law of absorption is applied for d and $DPF = 1$ as well as $l = d$.

Photon packet count was 10^9 per distance step and wavelength. The simulations were repeated five times with different seeds.

D. Wearable prototype and measurements

We developed a wearable prototype to record PPG curves with two LEDs (624 nm and 940 nm) as sources (see Fig. 2). The photodiode had a spectral sensitivity between 300 to 1100 nm. The cover glass had a transmission factor of 92% in the red and infrared spectral range. The refractive index was $n = 1.5$. The prototype was developed with four source-detector distances: 1.5, 3.0, 5.0, and 7.0 mm. The wearable was placed centrally on the phantom and the DC signal was recorded for 10 s at a frequency of 100 Hz. Measurements with the wearable prototype were repeated fives times.

E. Optical parameters

The optical parameters of the phantom, i.e. absorption and scattering coefficient, anisotropy factor, and refractive index, were previously characterised for wavelengths between 380 and 1400 nm [10], [11]. Table I summarises the key parameters.

TABLE I

OPTICAL PARAMETER OF THE LABORATORY SETUP.

Tissue	λ [nm]	μ_a $[mm^{-1}]$	μ_s' $[mm^{-1}]$	n [-]	g [-]
Glass slide	-	0.091 0.094 0.116	-	1.520	-
Air gap	-	-	-	1.000	-
Phantom	520 637 940	0.093 0.019 0.016	1.719 1.376 0.793	1.561 1.552 1.543	0.550

III. RESULTS

A. Laboratory Measurement

Figure 3 A-C shows measured DC level using the laboratory setup and detected photon weight derived from MC simulations across the band of source-detector distances. To compare measurements and simulations, signal levels are reported relative to their respective maximum at a source-detector distance d of 2.00 mm. As expected, received light decreased with increasing source-detector distance d for all wavelengths. The signal decrease was larger for measurements than simulations at 520 nm and smaller at 940 nm. At a wavelength of 637 nm, measurements and simulation showed a similar signal decrease. The deviation between measured and simulated signal was larger for at 520 nm than for the other wavelengths.

Absolute signal gradients across source-detector distance d are shown in Fig. 3 D-F. Absolute gradients decreased with increasing source-detector distance d. Gradients of simulated and measured data appeared similar at all wavelengths. With increasing source-detector distance d, measurement and simulation noise increased.

Figure 4 A shows that the differential pathlength factor DPF increased with increasing source-detector distance d for all wavelengths. DPF was larger at 637 nm than 940 nm. The DPF at 940 nm was smaller than at 520 nm up to a source-detector distance d of 2.6 mm. Mean maximum penetration depth increased with rising source-detector distance d (see Fig. 4 B). Photon packets at 940 nm penetrated the tissue deeper than at 637 nm and 520 nm.

There was no difference between detected photon weights for 10^8 and 10^9 simulated photon packets for short source-detector distances $d < 4.0$ mm, but thereafter the 10^8 photon packets simulation provides more varying estimates (see Fig. 5 A). As source-detector distance d increased, the shot noise to detected photon packets ratio increased too (see Fig. 5 B). The increasing noise effect was more pronounced for simulated data with 10^8 photon packets.

B. Wearable measurement

Figure 6 shows measured DC level of the wearable prototype attached to the phantom. As the diagram confirms, signal level decreased with increasing source-detector distance d. DC level at 624 nm decreased with a larger negative gradient than at 940 nm. Visually, measurements with the wearable device showed the same patterns for the relation

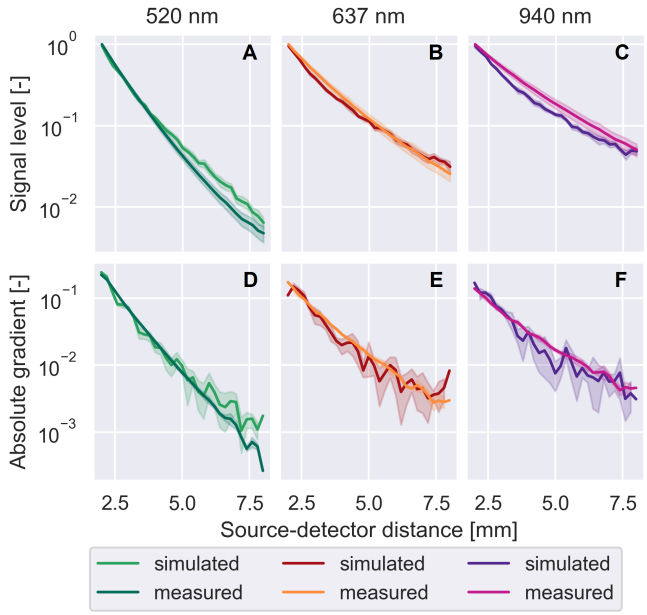

Fig. 3. A-C: Measured and simulated signal level per distance step and wavelength. D-F: Gradients of signal level per distance and wavelength.

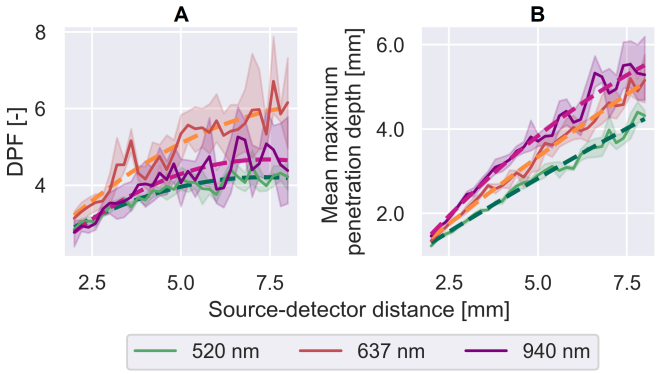

Fig. 4. A: Differential Pathlength Factor (DPF) of simulated data per distance and wavelength. B: Mean maximum penetration depth of simulated data per distance and wavelength.

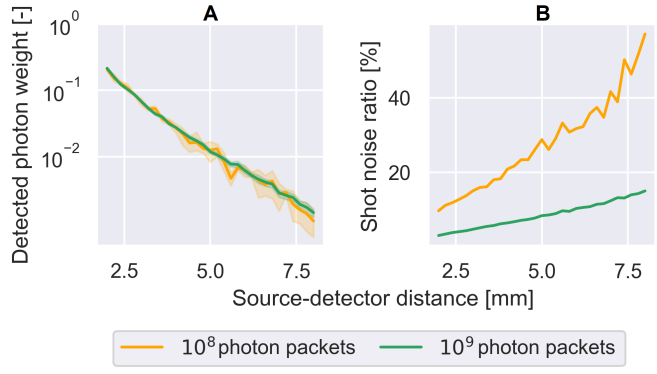

Fig. 5. Comparison of MC Simulation with 10^8 and 10^9 photon packets. A: Detected photon weight per source-detector distance d. B: Shot noise to detected photon packet ratio.

of signal level and source-detector distance d as observed in the laboratory measurements and in the simulations.

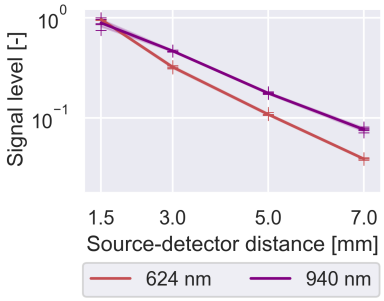

Fig. 6. Measured DC level of the wearable prototype attached to the phantom for varying source-detector distances d. Note that not all source-detector distances of the laboratory setup could be represented by the wearable prototype, see main text for details.

IV. DISCUSSION

As the source-detector distance d increased, so does the optical pathlength l of the detected photon packets due to scattering events in tissue. Detected photons pass through tissue in a banana-shaped curve [2]. Photon packets penetrated tissue deeper with increasing source-detector distance d, which can be seen by the increasing average maximum penetration depth and DPF which indicates a dependency between the two. With decreasing source-detector distance d, the dependency becomes more prominent. The information content and quality of the PPG curve depends on the tissue penetration depth. Consequently, the source-detector distance d has a direct influence on the PPG information. The differential pathlength factor DPF at 520 nm was lower than at 637 nm and the trend line at 940 nm was lower than at 637 nm, which confirms its wavelength dependency that was described before [12]. The DPF results are in agreement with analytical results, including the trend line crossing of 520 nm and 940 nm [13]. Moreover, we could reproduce the same effect with our wearable prototype at 624 nm and 940 nm.

Increasing source-detector distance d also increases simulation noise. With rising source-detector distance d less photon packets hit the detector and results of simulation runs varied more. Figure 5 B shows an increasing noise ratio for an increasing source-detector distance d. To reduce noise, the number of photon packets must be increased at the expense of computation time. The number of photon packets must be balanced between computation time and accuracy of simulation results. Figure 5 A shows that for a visual interpretation, 10^9 photon packets were sufficient.

The mean maximum penetration depth slopes of all wavelengths indicate a saturation point of the penetration depth (Fig. 4 B), which was shown by [14].

Measurements and simulations showed a substantial agreement, thus we were able to reproduce important effects in measurements by MC simulations. With increasing source-detector distance d, simulations showed an increasing deviation of the absorbed photon packet weights, which can be attributed to uncertainties of the longer optical pathlength l.

V. CONCLUSION

Reflective PPG DC signal level of a porcine skin phantom was measured in laboratory setting, with a wrist wearable prototype, and simulated within a MC framework. We could reproduce the dependency of DPF on source-detector distance d among measurements and simulations. Signal level dropped linearly in log-scale with increasing source-detector distance d. Source-detector distance d has an influence on the penetration depth, DPF, and PPG signal information content. The simulation can be used to investigate angle effects on the PPG signal and maximize the received signal. Thus the results are of interest for developing PPG wearables that are more robust to motion artifacts.

REFERENCES

[1] M. S. S. Johnson and J. Mikael Eklund, "A Review of Photoplethysmography-based Physiological Measurement and Estimation, Part 1: Single Input Methods," Jul. 2020, pp. 923–927. doi: 10.1109/EMBC44109.2020.9176353 .

[2] C. Mansouri and N. H., "New Window on Optical Brain Imaging; Medical Development, Simulations and Applications," in Selected Topics on Optical Fiber Technology, M. Yasin, Ed. InTech, 2012.

[3] T. Y. Abay and P. A. Kyriacou, "Reflectance Photoplethysmography as Noninvasive Monitoring of Tissue Blood Perfusion," IEEE Trans. Biomed. Eng., vol. 62, no. 9, pp. 2187–2195, Sep. 2015, doi: 10.1109/TBME.2015.2417863 .

[4] Y. Khan, D. Han, J. Ting, M. Ahmed, R. Nagisetty, and A. C. Arias, "Organic Multi-Channel Optoelectronic Sensors for Wearable Health Monitoring," IEEE Access, vol. 7, pp. 128114–128124, 2019, doi: 10.1109/ACCESS.2019.2939798 .

[5] T. Boonya-Ananta et al., "Synthetic photoplethysmography (PPG) of the radial artery through parallelized Monte Carlo and its correlation to body mass index (BMI)," Sci. Rep., vol. 11, no. 1, p. 2570, 28 2021, doi: 10.1038/s41598-021-82124-4 .

[6] C. Zhu and Q. Liu, "Review of Monte Carlo modeling of light transport in tissues," J. Biomed. Opt., vol. 18, no. 5, p. 050902, May 2013, doi: 10.1117/1 .JBO.18.5.050902 .

[7] T. Maeda, N. Arakawa, M. Takahashi, and Y. Aizu, "Monte Carlo simulation of spectral reflectance using a multilayered skin tissue model," Opt. Rev., vol. 17, no. 3, pp. 223–229, May 2010, doi: 10.1007/s10043-010-0040-5 .

[8] M. Reiser, A. Breidenassel and O. Amft, "Simulation framework for reflective PPG signal analysis depending on sensor placement and wavelength", 2022 IEEE 18th International Conference on Wearable and Implantable Body Sensor Networks, IEEE, 2022.

[9] P. Krauter et al., "Optical phantoms with adjustable subdiffusive scattering parameters," J. Biomed. Opt., vol. 20, no. 10, p. 105008, Oct. 2015, doi: 10.1117/1 .JBO.20.10.105008 .

[10] F. Foschum, F. Bergmann, and A. Kienle, "Precise determination of the optical properties of turbid media using an optimized integrating sphere and advanced Monte Carlo simulations. Part 1: theory," Appl. Opt., vol. 59, no. 10, p. 3203, Apr. 2020, doi: 10.1364/AO.386011 .

[11] F. Bergmann, F. Foschum, R. Zuber, and A. Kienle, "Precise determination of the optical properties of turbid media using an optimized integrating sphere and advanced Monte Carlo simulations. Part 2: experiments," Appl. Opt., vol. 59, no. 10, p. 3216, Apr. 2020, doi: 10.1364/AO.385939 .

[12] S. Chatterjee, T. Y. Abay, J. P. Phillips, and P. A. Kyriacou, "Investigating optical path and differential pathlength factor in reflectance photoplethysmography for the assessment of perfusion," J. Biomed. Opt., vol. 23, no. 07, p. 1, Jul. 2018, doi: 10.1117/1 .JBO.23.7.075005.

[13] F. Scholkmann and M. Wolf, "General equation for the differential pathlength factor of the frontal human head depending on wavelength and age," J. Biomed. Opt., vol. 18, no. 10, p. 105004, Oct. 2013, doi: 10.1117/1 .JBO.18.10.105004.

[14] S. Chatterjee, K. Budidha, and P. A. Kyriacou, "Investigating the origin of photoplethysmography using a multiwavelength Monte Carlo model," Physiol. Meas., vol. 41, no. 8, p. 084001, Sep. 2020, doi: 10.1088/1361-6579/ aba008 .